AGU PUBLICATIONS

JGR

Journal of Geophysical Research: Oceans

RESEARCH ARTICLE

10.1002/2017JC013453

Key Points:
- Inversion of constituent concentrations from in situ measurements of inherent optical properties in complex waters
- Local material-specific inherent optical properties derived by linear regression of partitioned data set into optically dominant constituent
- Special attention is paid to different sources of measurement uncertainties and error propagation through the inversion model

Correspondence to:
M. Ramírez-Pérez,
mramirez@icm.csic.es

Citation:
Ramírez-Pérez, M., Twardowski, M., Trees, C., Piera, J., & McKee, D. (2018). Inversion of in situ light absorption and attenuation measurements to estimate constituent concentrations in optically complex shelf seas. *Journal of Geophysical Research: Oceans*, *123*, 720–737. https://doi.org/10.1002/2017JC013453

Received 12 SEP 2017
Accepted 3 JAN 2018
Accepted article online 9 JAN 2018
Published online 30 JAN 2018

The copyright line for this article was changed on 10 APR 2018 after original online publication.

Inversion of In Situ Light Absorption and Attenuation Measurements to Estimate Constituent Concentrations in Optically Complex Shelf Seas

M. Ramírez-Pérez[1], M. Twardowski[2], C. Trees[3], J. Piera[1], and D. McKee[4]

[1]Physical and Technological Oceanography Department, Institute of Marine Sciences, Barcelona, Spain, [2]Harbor Branch Oceanographic Institute, Florida Atlantic University, Ft. Pierce, FL, USA, [3]Research Department, Centre for Maritime Research and Experimentation, La Spezia, Italy, [4]Physics Department, University of Strathclyde, Glasgow, UK

Abstract A deconvolution approach is presented to use spectral light absorption and attenuation data to estimate the concentration of the major nonwater compounds in complex shelf sea waters. The inversion procedure requires knowledge of local material-specific inherent optical properties (SIOPs) which are determined from natural samples using a bio-optical model that differentiates between Case I and Case II waters and uses least squares linear regression analysis to provide optimal SIOP values. A synthetic data set is used to demonstrate that the approach is fundamentally consistent and to test the sensitivity to injection of controlled levels of artificial noise into the input data. Self-consistency of the approach is further demonstrated by application to field data collected in the Ligurian Sea, with chlorophyll (*Chl*), the nonbiogenic component of total suspended solids (TSS_{nd}), and colored dissolved organic material (*CDOM*) retrieved with RMSE of 0.61 mg m^{-3}, 0.35 g m^{-3}, and 0.02 m^{-1}, respectively. The utility of the approach is finally demonstrated by application to depth profiles of in situ absorption and attenuation data resulting in profiles of optically significant constituents with associated error bar estimates. The advantages of this procedure lie in the simple input requirements, the avoidance of error amplification, full exploitation of the available spectral information from both absorption and attenuation channels, and the reasonably successful retrieval of constituent concentrations in an optically complex shelf sea.

1. Introduction

There is great interest in characterizing water quality over a wide range of spatial and temporal scales in shelf seas. In situ optical sensors are ideally suited to be deployed on a variety of platforms including moorings, AUVs and from ships (Boss et al., 2007; Nelson et al., 1998; Smith & Baker, 1978; Stramski et al., 1999; Twardowski et al., 2005) to provide data sets with high spatiotemporal resolution. The optical properties of natural waters are controlled by the concentration and type of constituents present in the water which includes: phytoplankton and associated biogenic detritus (usually related to chlorophyll *a* concentration, *Chl*), nonbiogenic suspended solids (often classed as mineral suspended solids, *MSS*, but see below for discussion of limitations in this assumption) and colored dissolved organic material, *CDOM* (Kirk, 1994).

The potential to derive information about constituent characteristics from measured inherent optical properties (IOPs) has motivated many studies, which focus on the estimation of primary productivity (Huot et al., 2007; Lee et al., 2011), particle matter concentration (Boss et al., 2009; Groundwater et al., 2012; Hill et al., 2011; Neukermans et al., 2012) and size distribution (Astoreca et al., 2012; Boss et al., 2001), particle density (McKee & Cunningham, 2006; Twardowski et al., 2001, 2012), phytoplankton groups (Eisner et al., 2003; Torrecilla et al., 2011), or particulate carbon (Gardner et al., 2001; Loisel et al., 2001; Stramski et al., 1999). However, quantification of the major nonwater constituent concentrations from these measurements is still a challenging task because simple relationships vary locally with particle composition; thus a generally accepted protocol does not yet exist (Brown et al., 2007). The most direct method to address this issue is by means of the material-specific IOPs (SIOPs), since these parameters provide a link between IOPs and concentrations of the materials in water. While this may seem straightforward, there is in fact a significant challenge in generating all of the required SIOPs as this requires (a) a suitable bio-optical model to relate available optical and biogeochemical measurements and (b) ability to partition IOP data into constituent-related components

(e.g., McKee & Cunningham, 2006; Zheng & Stramski, 2013). This is partly achieved by ancillary measurements and laboratory analysis, such as filter pad spectrophotometry (to separate the absorption by phytoplankton and by nonalgal particulate material) and absorption measurements of 0.2 μm filtered seawater (for deriving the absorption by CDOM). However, there is not at present any technique to separate particulate scattering and nonalgal particulate absorption into biogenic and nonbiogenic components. This has led some authors to determine the SIOPs based on (1) multiple linear regression of total IOPs against constituent concentrations (Brown et al., 2007; Strömbeck et al., 2004), (2) simple linear regression for data sets partitioned by optically dominant constituent (McKee & Cunningham, 2006), or (3) laboratory analysis of phytoplankton cultures (Bricaud et al., 1983; Stramski & Morel, 1990) and purified suspended minerals (Babin & Stramski, 2002, 2004). The linear regression analysis proposed by McKee and Cunningham (2006) allows calculation of representative SIOPs for a specific location and is attractive as the method reduces the impact of systematic and random errors (McKee et al., 2014). These authors used relationships between IOPs to identify optically distinct water types dominated by different constituents (*Chl* or *MSS*) in the studied area, which allowed the application of regression analysis to partitioned IOPs and single constituent concentrations. As there is not a simple one-to-one correspondence between observed IOPs and relevant biogeochemical constituents, determination of local SIOPs inevitably involves pragmatic decisions on how to partition in situ data.

It is important to highlight that the regression analyses discussed above consider linear relationships between IOPs and constituent concentration. This is a simplification which requires careful consideration. For example, it is well known that the chlorophyll-specific phytoplankton absorption coefficient decreases with increasing *Chl* concentration due to the pigment packaging effect (Bricaud et al., 1995). However, it is proposed here that linear regression can be performed for the ranges of chlorophyll concentration values that are relevant for shelf seas as the effect of pigment packaging will be relatively limited for these values. This obviously places a constraint over the general applicability of such an approach, but this should be viewed as a pragmatic decision that results from the need to deal with several competing requirements and the emphasis on using deconvolution for optically complex shelf waters. For comparison, a recent paper presented a nonlinear bio-optical model based on the same data set (Bengil et al., 2016). However, incorporating this into the current deconvolution method would involve adoption of significantly more complex numerical solver techniques and is beyond the scope of this paper.

There are different approaches to invert in situ IOPs measurements without using SIOPs. For example, Gallegos and Neale (2002) employed normalized absorption spectra in a matrix inversion approach, while Schofield et al. (2004) developed a nonlinear constrained regression of bulk absorption spectra. However, these methods provide estimates of optical weights and spectral slopes for the different constituents rather than values of concentrations.

For these reasons, the focus of this study is on developing a simple IOP inversion model based on knowledge of local SIOPs. This model utilizes all the spectral information contained in in situ absorption and attenuation data to retrieve the major nonwater compound concentrations in complex shelf sea areas. SIOPs are determined from a limited number of natural samples, following an extended version of the McKee and Cunningham (2006) approach, and special attention has been paid to the impact of different sources of uncertainties in the retrieval.

2. Theory

2.1. A Linear Spectral Deconvolution Model for Inversion of In Situ AC-9 Data

The total absorption and scattering coefficients can be written as the sum of the corresponding coefficients of individual components:

$$a(\lambda)=a_{ph}(\lambda)+a_{bd}(\lambda)+a_{nd}(\lambda)+a_{CDOM}(\lambda)+a_w(\lambda) \quad (1)$$

$$b(\lambda)=b_{ph}(\lambda)+b_{nd}(\lambda)+b_w(\lambda) \quad (2)$$

where the subscripts represent the following: phytoplankton (*ph*), biogenic detritus (*bd*), nonbiogenic detritus (*nd*), colored dissolved organic material (*CDOM*), and water (*w*). This slightly awkward formulation is necessary in order to facilitate subsequent integration with measured parameters. In particular, biogenic detrital scattering is included in the phytoplankton scattering term (b_{ph}) as it is currently not possible to

separate these experimentally or numerically. Equations (1) and (2) can be expressed as the product of SIOPs and constituent concentrations:

$$a(\lambda)=a^*_{ph}(\lambda)\,Chl+a^*_{bd}(\lambda)\,Chl+a^*_{nd}(\lambda)\,TSS_{nd}+a^*_{CDOM}(\lambda)\,CDOM+a_w(\lambda) \tag{3}$$

$$b(\lambda)=b^*_{ph}(\lambda)\,Chl+b^*_{nd}(\lambda)\,TSS_{nd}+b_w(\lambda) \tag{4}$$

where the constituent concentrations are as follows: chlorophyll (*Chl*), the nonbiogenic detrital component of total suspended solids (TSS_{nd}), and the absorption of *CDOM* at 440 nm. $a^*_{CDOM}(\lambda)$ is actually the *CDOM* absorption spectrum normalized to the signal at 440 nm. It is assumed (e.g., Morel, 1988) that biogenic variables covary with *Chl*.

In order to combine available information for each wavelength, the scattering to absorption ratio is used:

$$\frac{b(\lambda)}{a(\lambda)}=\frac{b^*_{ph}(\lambda)\,Chl+b^*_{nd}(\lambda)\,TSS_{nd}+b_w(\lambda)}{a^*_{ph}(\lambda)\,Chl+a^*_{bd}(\lambda)\,Chl+a^*_{nd}(\lambda)\,TSS_{nd}+a^*_{CDOM}(\lambda)\,CDOM+a_w(\lambda)} \tag{5}$$

The equation can be simplified, grouping terms to *Chl*, TSS_{nd}, and *CDOM*, as follows:

$$\begin{aligned}\left[b(\lambda)a^*_{ph}(\lambda)-a(\lambda)b^*_{ph}(\lambda)+b(\lambda)a^*_{bd}(\lambda)\right]Chl+\left[b(\lambda)a^*_{nd}(\lambda)-a(\lambda)b^*_{nd}(\lambda)\right]TSS_{nd}\\ \cdots+\left[b(\lambda)a^*_{CDOM}(\lambda)\right]CDOM=-b(\lambda)a_w(\lambda)+a(\lambda)b_w(\lambda)\end{aligned} \tag{6}$$

The total absorption and scattering coefficients, $a(\lambda)$ and $b(\lambda)$, the SIOPs and the absorption and scattering of pure water, $a_w(\lambda)$ and $b_w(\lambda)$, are all known. $a_w(\lambda)$ and $b_w(\lambda)$ are taken from Pope and Fry (1997) and Morel (1974), respectively. These coefficients are also added to the AC-9 measurements to obtain the total absorption and scattering coefficients, $a(\lambda)$ and $b(\lambda)$. The inclusion of water terms is necessary to avoid formation of homogeneous systems of equations (all equations equal zero) which do not have single, nontrivial solutions. The chlorophyll, nonbiogenic detrital suspended sediments, and *CDOM* concentrations (*Chl*, TSS_{nd}, and *CDOM*, respectively) are unknowns and are found by minimizing least squares for n wavelengths, where $n \geq 3$. In this case, the system is formed by nine equations ($n = 9$), corresponding to the nine available AC-9 wave bands. For oceanic waters (Case I waters) where the optical properties are dominated by algae and covarying materials, the inversion model is reduced to two unknowns: *Chl* and *CDOM*.

2.2. Practical Implementation of the Spectral Deconvolution Model

In Case I waters, it is assumed that the nonbiogenic detrital components of absorption and scattering are negligible. Consequently, for Case I waters, nonalgal particulate absorption, $a_{NAP}(\lambda)$, measured using bleached filter pads is classed here as biogenic detrital absorption, $a_{bd}(\lambda)$, and is assumed to correlate with *Chl* (and is demonstrated as such later). The corresponding SIOP, $a^*_{bd}(\lambda)$, can therefore be determined by simple linear regression. In Case II waters, $a_{NAP}(\lambda)$ is assumed to have both biogenic and nonbiogenic components. However, the biogenic component can be established from associated *Chl* and Case I estimates of $a^*_{bd}(\lambda)$ and the nonbiogenic component of NAP absorption is then given by

$$a_{nd}(\lambda)=a_{NAP}(\lambda)-a^*_{bd}(\lambda)\,Chl \tag{7}$$

A similar argument allows partitioning of the Case II particulate scattering coefficient, $b_p(\lambda)$, into biogenic and nonbiogenic components using

$$b_{nd}(\lambda)=b_p(\lambda)-b^*_{ph}(\lambda)\,Chl \tag{8}$$

where the chlorophyll-specific phytoplankton scattering coefficient, $b^*_{ph}(\lambda)$, is previously determined for Case I waters using linear regression of $b_p(\lambda)$ against *Chl*, and includes contributions for all biogenic particles found in Case I waters. Finally, it is necessary to relate these two nonbiogenic detrital IOPs to the nonbiogenic detrital mass concentration, TSS_{nd}. Unfortunately, this cannot be directly measured. In Case I waters, the total suspended solids concentration, *TSS*, can be assumed to be biogenic in origin, while in Case II waters there will also be a nonbiogenic component. While combustion of filtered material to give mineral suspended solids, *MSS*, will remove the organic content, it will leave biogenic minerals such as diatom frustules on the filter paper. In this case, it is suggested that establishing a relationship between *TSS* and *Chl* for Case I waters permits subsequent estimation of the biogenic component of *TSS* for Case II waters using

$$TSS_{nd} = TSS - TSS^{*}_{bd}\, Chl \quad (9)$$

This partitioning approach has previously been successfully demonstrated for this data set by Bengil et al. (2016), who used this data set to establish a bio-optical model for the Ligurian Sea, adopting full nonlinear fits to maximize the range of compatibility. In this paper, however, it is necessary to limit the analysis to linear fits between IOPs and constituent concentrations as the deconvolution model is solved as a system of linear equations. An advanced version, incorporating nonlinear SIOP models is planned for the future but requires significantly more complex mathematical solving processes.

2.3. Propagation of Measurement Uncertainty

A key benefit of the proposed spectral deconvolution approach is the computational simplicity of solving a system of linear equations. At the same time, there is a need to consider how uncertainties in both IOPs and SIOPs propagate through the model and the system is sufficiently complex that an analytical approach is unattractive. Under these circumstances it is suggested that statistical bootstrapping is an efficient means of assessing the propagation of errors (Davison & Hinkley, 1997). To do this, it is necessary to establish uncertainty estimates for both IOPs and SIOPs, taking care to consider both the magnitude and the nature (e.g., absolute versus fractional) of the uncertainties. Once these are available, it is a simple matter of injecting randomly distributed errors into observations and repeatedly solving the system of equations to build up statistical distributions of constituents. The final outcome is a set of constituent concentrations that are quantified as a best estimate (median) and associated uncertainty (standard deviation of the bootstrap distribution). The ability to rapidly establish associated uncertainties in the constituent concentrations is a particularly useful aspect of this approach.

3. Materials and Methods

3.1. Field Data

Sampling was performed at 60 stations in the Ligurian Sea, off the northwest coast of Italy, between 13 and 26 March 2009 on the RV Alliance during the BP09 cruise, with a total of 36 stations returning complete data sets after full quality control. Stations can be classified in two different groups according to location: offshore and onshore with 12 and 24 stations, respectively (Figure 1). The first group was characterized by deep (up to 2,500 m) oceanic waters where a spring bloom was occurring, whereas the second group belonged to the shallow coastal region, ranging from quite clear to turbid waters, including some stations within the plume of the River Arno. More detailed information about the study area can be found in McKee et al. (2014). At each station, vertical profiles of spectral absorption and attenuation coefficients were measured and water samples were collected simultaneously at different depths for later laboratory analysis.

3.2. In Situ Optical Measurements

Vertical profiles of the total nonwater absorption (a_{nw}) and beam attenuation (c_{nw}) coefficients were measured in situ with a WET Labs 25 cm path length AC-9 instrument operating at nine wavelengths across the visible-NIR (412, 440, 488, 510, 532, 555, 650, 676, and 715 nm, 10 nm FWHM) and data were averaged over 1 m depth intervals. AC-9 measurements were calibrated during the cruise with ultrapure water (Milli-Q, Millipore) and the salinity and temperature dependence of pure water were corrected in all samples (Pegau et al., 1997) using data from a Seabird SBE 19 plus CTD. The proportional correction by Zaneveld et al. (1994) was used to correct AC-9 absorption data for scattering collection errors. In situ backscattering measurements were made with a BB9 backscattering meter (WET Labs Inc.) operating at 412, 440, 510, 532, 595, 660, 676, and 715 nm. BB9 data were linearly interpolated where necessary to match AC-9 wavelengths and were corrected for temperature, salinity and path length absorption effects in line with the manufacturer's instructions. Particulate scattering b_p was derived from $c_{nw} - a_{nw}$. Total absorption (a) and scattering (b) values were obtained by adding pure water values, $a_w(\lambda)$ and $b_w(\lambda)$, from Pope and Fry (1997) and Morel (1974), respectively. Note the c measurement has an acceptance angle of 0.9°, so these c and b parameters do not include scattering in the 0°–0.9° solid angle. The AC-9 was deployed from the surface to the maximum depth possible in shallow stations or down to a maximum of 100 m for deeper stations.

3.3. Laboratory Measurements

The absorption of all dissolved and suspended components minus water was measured using a Point Source Integrating Cavity Absorption Meter (PSICAM; Röttgers & Doerffer, 2007; Röttgers et al., 2005, 2007).

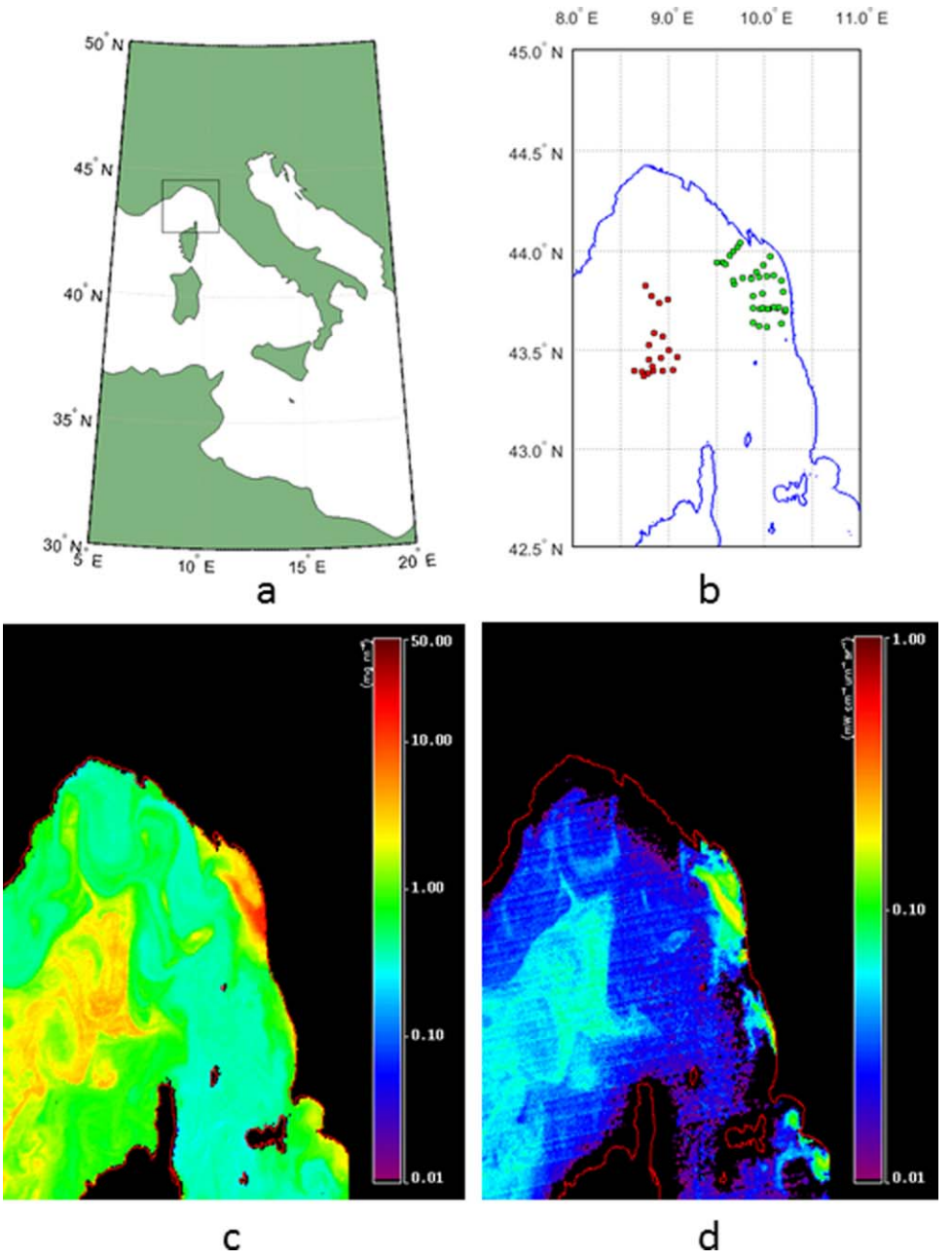

Figure 1. Description of the study area. (a) Study area marked within box and (b) location of offshore (circles) and onshore (squares) stations for the BP09 cruise. (c) MODIS standard *Chl* from 18 March 2009 shows a bloom in the central region of the Ligurian Sea, northwest of Corsica. The high intensity "bloom" on the Italian coast is actually a sediment plume from the River Arno, which is clearly identified from (d) MODIS *nLw667* from the same date.

This instrument has previously been extensively validated and has been shown to provide high accuracy (±2%) absorption coefficients across a wide range of water conditions. A 1 m liquid waveguide capillary cell (LWCC) with an Ocean Optics USB2000 minispectrometer was used to measure absorption by CDOM. This instrument is somewhat faster to operate than the PSICAM and provides noise range of $\pm 0.0001\ m^{-1}$ (95% Prediction Interval) at 532 nm. In both cases, measurements were made against fresh Milli-Q references and all samples were corrected for the effects of salinity and temperature on water absorption (Röttgers & Doerffer, 2007). From this pair of measurements, particulate absorption, $a_p(\lambda)$, was derived by subtraction of CDOM absorption, a_{CDOM}, from PSICAM nonwater absorption, a_{PSICAM}.

In addition, total particulate absorption, $a_p(\lambda)$, was also measured using the quantitative filter pad method (Ferrari & Tassan, 1999). Samples were placed directly in front of the optical windows of a Shimadzu UV-2501 PC spectrophotometer. Absorption by phytoplankton, $a_{ph}(\lambda)$, was determined by bleaching samples, measuring the absorption of nonalgal particles, $a_{NAP}(\lambda)$, and subtracting this from $a_p(\lambda)$. Path length amplification factors and scattering offset corrections were determined using a linear regression approach (Lefering et al., 2016; McKee et al., 2014) and corresponding PSICAM $a_p(\lambda)$ data. The resulting filter pad corrections were subsequently applied to both bleached and unbleached filter pad absorption spectra.

Chlorophyll concentration was measured using standard HPLC measurements on samples filtered through GF/F filters, stored in liquid nitrogen and transported to laboratories for later analysis. *Chl* data presented here were collected by colleagues from Management Unit of the North Sea Mathematical Models (MUMM). Triplicate HPLC samples were analyzed by the Marine Chemistry Laboratory of the MUMM using a reversed phase, acetone-based method with a C18 column and a Jasco FP-1520 fluorescence detector. In this paper, *Chl* refers to the chlorophyll a concentration and does not include contributions from other pigments.

Total suspended solids concentrations (*TSS*) were obtained by colleagues from MUMM by filtering samples through preashed, rinsed and preweighed 47 mm GF/F filters. Samples were rinsed with several aliquots of ultrapure water, taking care to rinse the edge of the filter to minimize salt retention. Filters were stored frozen and returned to the lab where they were dried and reweighed. All samples were measured in triplicate and final values expressed as averages.

4. Results

Having established a conceptual framework for the spectral deconvolution approach, the aim of what follows is to demonstrate the feasibility of its parameterization and then to establish theoretical and practical performance. The stages of model development are therefore as follows:

1. Determine an appropriate water classification scheme for the Ligurian Sea data set to support partitioning of IOPs and TSS.
2. Determine spectral SIOPs required for incorporation into equation (4). In the same process, determine associated SIOP uncertainties for inclusion into bootstrapping.
3. Establish theoretical performance for the deconvolution approach using a synthetic data set and bootstrapping to determine the effect of measurement uncertainty propagation.
4. Establish practical performance using the set of in situ IOPs and associated biogeochemical data from the Ligurian Sea.
5. Demonstrate ability to convert AC-9 depth profiles into constituent concentration depth profiles.

4.1. Water Type Classification

The Ligurian Sea data set consists of two geographically separated subsets. The offshore data set was collected in deep oceanic waters that are assumed to be Case I optically. The onshore data set crosses the continental shelf into coastal waters where the influence of nonbiogenic material becomes significant and the water fits a Case II classification. Across the entire data set *Chl* varied between 0.29 and 3.31 mg m^{-3}, *TSS* varied from 0.13 to 3.77 mg L^{-1}, and *CDOM* varied from 0.01 to 0.1 m^{-1} (at 440 nm). The distinction in optical and biogeochemical properties between onshore and offshore waters is illustrated in Figure 2. Offshore stations show significantly lower particulate backscattering ratios (Figure 2a) and also lower values of *TSS:Chl*, both reflecting the increased significance of nonbiogenic particles for onshore stations. A best fit linear regression forced through the origin provides an estimate of TSS^*_{bd} required for equation (9). Although there is significant spread in the data, the dashed lines provide 95% confidence intervals for this value. The question then is to what extent can this relationship be expected to work for the biogenic component of the onshore particulate population? This will largely be determined by the consistency of the phytoplankton population across the two subsets of data. Figure 3a shows 440 nm normalized phytoplankton absorption spectra for the entire data set. There is remarkably little variability in the shape of these spectra, supporting the idea that the phytoplankton properties are relatively consistent across both subsets. In this case, it seems reasonable to assume that the broader biogenic properties are likely to be similarly consistent. Based on this, it will be reasonable to determine chlorophyll-specific absorption coefficients for phytoplankton, $a^*_{ph}(\lambda)$, using the entire data set. Similarly, Figure 3b shows 440 nm normalized *CDOM* absorption

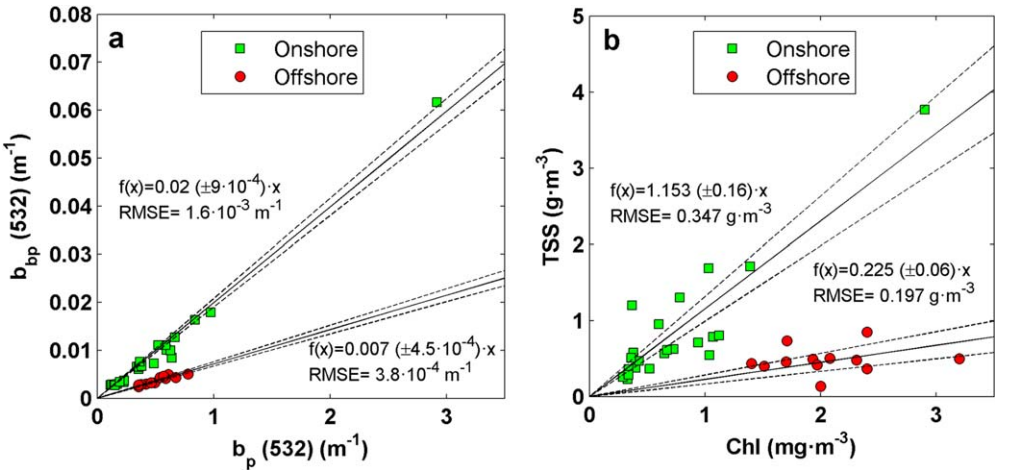

Figure 2. (a) Particulate backscattering against particulate scattering at 532 nm and (b) *Chl* against total suspended matter concentration (*TSS*) for all the stations from Ligurian Sea. Offshore and onshore stations marked with red circles and green squares, respectively. Black solid and dashed lines represent the best fit line forced through origin and ±95% confidence bounds.

spectra for the entire data set, with very little obvious difference in spectral structure across the data set. Based on this, it is also reasonable to use the entire data set to establish a single normalized *CDOM* absorption spectrum, $a^*_{CDOM}(\lambda)$.

4.2. Determination of SIOPs and Associated Uncertainties

The set of material-specific absorption and scattering coefficients required to populate the spectral deconvolution model (equation (6)) was derived by linear least squares regression of partitioned IOPs against associated constituent concentrations from surface water samples (Figure 4). Regressions were applied for each available wavelength and were forced through the origin to avoid the complicating influence of statistical offsets. Following McKee et al. (2009, 2014), the regression slopes were taken as the optimal SIOP values, and the 95% confidence intervals in these slopes, $CI_{95\%}$, were considered to represent the uncertainty in each SIOP. $CI_{95\%}$ were calculated as 1.96σ and were included in the inversion procedure to quantify the product uncertainties.

As there does not appear to be significant variability in the spectral structure of $a_{ph}(\lambda)$ or $a_{CDOM}(\lambda)$ across the data set (Figure 3), the corresponding SIOPs could be derived using both the Case I and Case II parts of the data set (Figures 4a and 4b). Coefficients of determination (R^2) for $a^*_{ph}(\lambda)$ were 0.9 on average. Ninety-

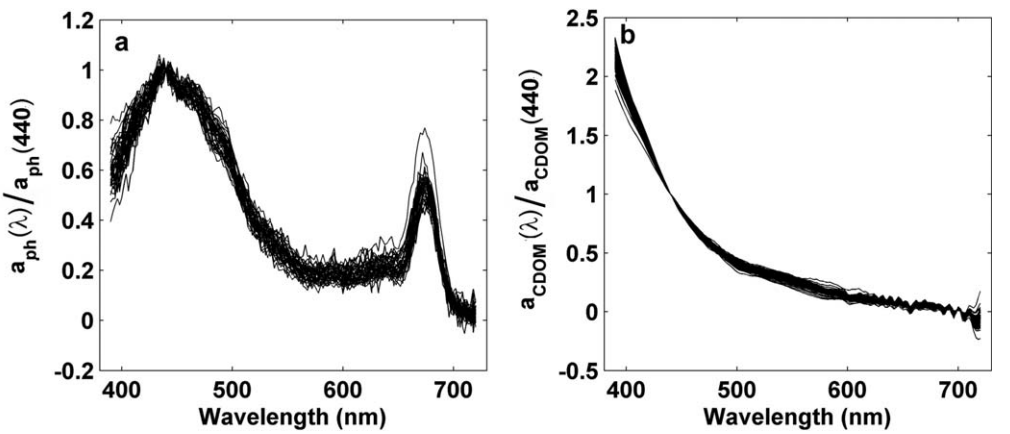

Figure 3. Variability on phytoplankton and CDOM absorption spectra. (a) Phytoplankton absorption spectra normalized at 440 nm show very little spectral variability across the entire data set. (b) 440 nm normalized *CDOM* spectra are also very consistent across the entire data set.

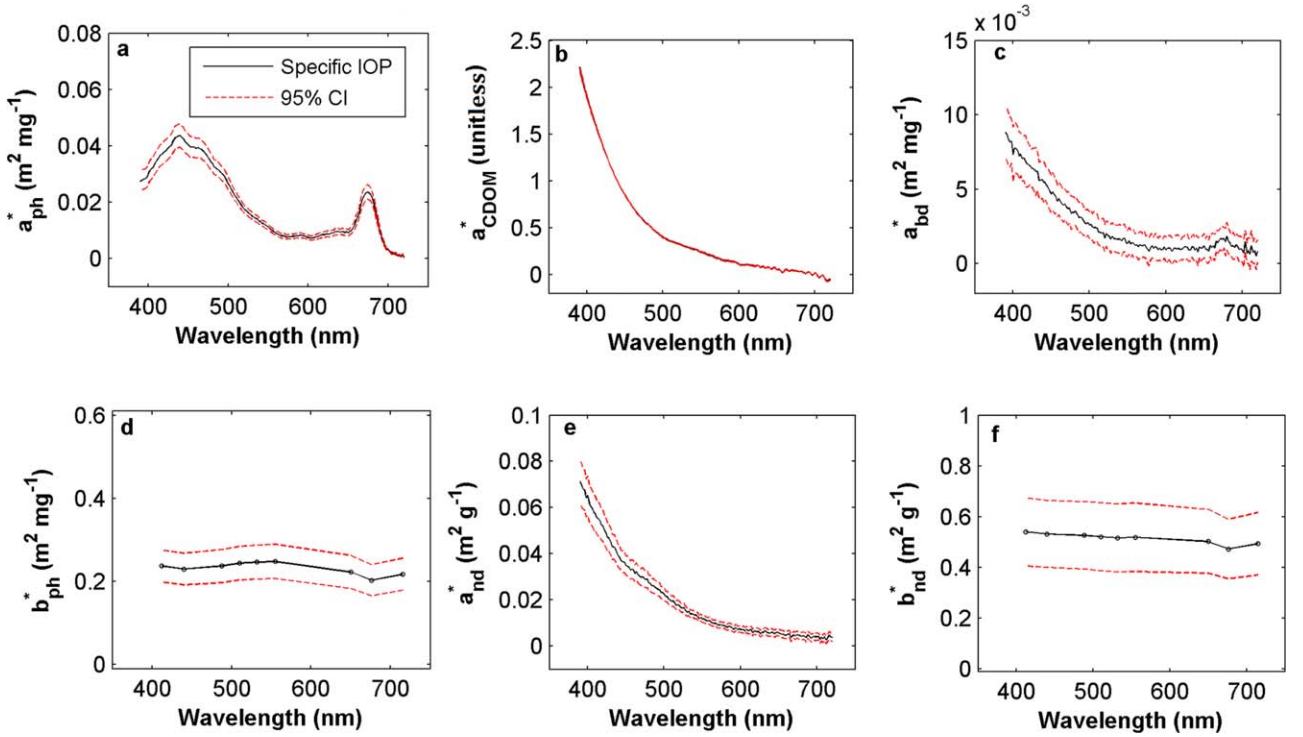

Figure 4. Material-specific IOPs with 95% confidence bounds obtained by linear regression: (a) *Chl*-specific phytoplankton absorption—full data set, (b) *CDOM* absorption normalized at the signal at 440 nm—full data set, (c) *Chl*-specific biogenic detrital absorption—offshore data set, (d) *Chl*-specific phytoplankton scattering—offshore data set, (e) TSS_{nd}-specific nonbiogenic detrital absorption coefficient—onshore data set, and (f) TSS_{nd}-specific nonbiogenic detrital scattering coefficient—onshore data set.

five percent confidence intervals varied across the spectrum but were generally narrow (maximum $\sim$ 0.01 m^2 mg^{-1}) and represented less than fifteen percent of the slope value for $\lambda < 700$ nm. This linearly derived single $a^*_{ph}(\lambda)$ spectrum can be justified by noting that *Chl* varied from 0.3 to 3.3 mg m^{-3} and that over this range the power law function proposed by Bricaud et al. (1995) can reasonably be approximated with a linear function. Linear regressions for $a^*_{CDOM}(\lambda)$ had an average $R^2 = 0.95$ with $CI_{95\%} < 5\%$ of corresponding signal for the majority of wavelengths.

Biogenic detrital absorption and chlorophyll-specific scattering SIOPs were derived using data from offshore stations only, assuming that these were effectively Case I waters. Figures 4c and 4d show $a^*_{bd}(\lambda)$ and $b^*_{ph}(\lambda)$, respectively, obtained by regression of $a_{NAP}(\lambda)$ and $b_p(\lambda)$ against *Chl* for the offshore data set. Coefficients of determination for $a^*_{bd}(\lambda)$ were >0.85 for $\lambda < 500$ nm but decreased with increasing wavelength. This is a natural consequence of the signal decreasing with wavelength. 95% confidence intervals for $a^*_{bd}(\lambda)$ were broadly constant at approximately $\pm$0.002 m^2 mg^{-1} across the spectrum. A small peak centered on 676 nm indicates the presence of residual quantities of algal pigment due to imperfect bleaching of filters. The $b^*_{ph}(\lambda)$ spectrum shows features associated with anomalous dispersion around pigment absorption peaks. Coefficients of determination were >.93 across the spectrum and $CI_{95\%}$ were consistent across the spectrum at $\pm$0.04 m^2 mg^{-1}.

The nonbiogenic component of total suspended solids concentration (TSS_{nd}) for onshore stations was obtained using equation (9) and the value of TSS^*_{bd} obtained from Figure 2b. Similarly, nonbiogenic components of detrital absorption, $a_{nd}(\lambda)$, and particulate scattering, $b_{nd}(\lambda)$, were obtained for onshore stations using equations (7) and (8) and biogenic SIOPs determined for offshore stations. Nonbiogenic detrital SIOPs, $a^*_{nd}(\lambda)$ and $b^*_{nd}(\lambda)$, were obtained by correlating associated IOPs with TSS_{nd}. Figure 4e shows the resulting $a^*_{nd}(\lambda)$ spectrum, with the signal decreasing approximately exponentially with wavelength as expected, though there is a small, broad feature around 480 nm that might be imperfect pigment bleaching or, alternatively an unknown mineral absorption feature. Despite the additional level of processing required to reach this stage, the coefficient of determination gave an average $R^2 = 0.84$ across all wavelengths. $CI_{95\%}$

values decreased with increasing wavelength with maximum values of ~0.01 $m^2\ g^{-1}$ in the blue. $b^*_{nd}(\lambda)$ was featureless and showed only a small decrease with wavelength (Figure 4f). However, this masks the fact that this set of regressions returned the lowest coefficients of determination with average $R^2 > 0.75$ across the spectrum. Normalized nonbiogenic detrital scattering spectra showed a broader range of spectral variability than any of the other IOPs in this data set. $CI_{95\%}$ values were spectrally invariant however, with an average value of $\pm 0.15\ m^2\ g^{-1}$.

4.3. Spectral Deconvolution Model Sensitivity Analysis

The spectral deconvolution model represented by equation (6) is a system of linear equations operating on spectrally dependent IOPs and SIOPs to retrieve three unknown constituent concentrations: *Chl*, TSS_{nd}, and *CDOM*. In the case of AC-9 data, there are nine available spectral bands, providing an overdetermined system of equations that can nevertheless be easily solved in Matlab (The Mathworks, Inc.) using the *mldivide* operator that provides a least squares solution. This approach enables exploitation of all of the spectral information provided by the AC-9 sensor combination. The aim of this sensitivity analysis is to establish basic algorithm performance in the case of perfect input data and then to determine the impact of measurement uncertainties (and other sources of variability). By its nature, this is an open-ended problem so the analysis will be restricted to set ranges of constituent concentrations and a single set of measurement uncertainty ranges.

Synthetic IOPs were generated based on SIOPs derived in the previous section and different combinations of constituent concentrations according to equations (3) and (4). The synthetic IOP data set comprised 1,000 absorption and scattering coefficient spectra modeled using log-spaced constituent concentrations between specific ranges. Concretely, *Chl* ranged from 0.01 to 100 mg m^{-3}, TSS_{nd} from 0.1 to 100 g m^{-3}, and *CDOM* from 0.01 to 10 m^{-1}. AC-9 measurement uncertainties were modeled as normally distributed random values with a standard deviation $\sigma = \pm 0.0025\ m^{-1}$ corresponding to the manufacturer's estimates of the instrument precision ($\pm 0.005\ m^{-1}$). These errors were assumed to be absolute in magnitude (consistent with McKee et al., 2009) and random with wavelength, so a separate error was generated for each wavelength and measurement of absorption and attenuation. Uncertainties in SIOPs were expressed as normally distributed random errors within the range ±5%. This arbitrary value was selected as being broadly representative of the 95% confident intervals obtained from linear regressions in the previous section. A relative error was selected for the SIOPs to reflect the apparent dependence on signal observed in, e.g., Figure 4a. Note, however, that this is a simplification only used for this sensitivity analysis. For each combination of constituents, 1,000 sets of IOPs with randomly generated errors were created and propagated through the deconvolution model to produce distributions of constituent concentration estimates. The median minus the input value was used to quantify the offset error while the spread in the retrieved values was expressed as the standard deviation of the output distributions.

The magnitude of the offset error was typically of the order of 10^{-2} to 10^{-3} (relevant units for each parameter) and only increased to significant levels when each constituent reached the very highest end of the simulated ranges. For the constituent concentration ranges in the Ligurian Sea data set, the offset error can be assumed to be negligible. Figure 5 shows the spread and offset errors in retrieval of *Chl* for all combinations of constituent concentrations for three different scenarios: (a and b) zero error in both IOPs and SIOPs, (c and d) zero error in IOPs and 5% error in SIOPs, and (e and f) $\sigma = \pm 0.0025\ m^{-1}$ error in IOPs and zero error in SIOPs. Retrieval of constituents when the input errors are zero (Figures 5a and 5b) is effectively perfect for the synthetic data set. This is to be expected and is merely confirmation that the Matlab *mldivide* operator is successfully dealing with the overdetermined system of equations. Introducing relative errors into the SIOPs and absolute errors into the IOPs impact differently on the distribution of retrieved *Chl*. The effect of a 5% relative error in SIOPs results in a spread error distribution that effectively scales with the magnitude of the constituent concentrations, though CDOM does not appear to be particularly significant (Figure 5c). Introduction of the 5% SIOP error results in offset errors in the distribution of output *Chl* values that increase as the concentration gets smaller and, somewhat unexpectedly, are skewed toward underestimates (Figure 5d). The effect of an absolute error in IOPs, on the other hand, is more evenly spread and potentially more significant at low concentrations for both spread and offset errors (Figures 5e and 5f). The salient point is that it is essential that both the *magnitude* and the *nature* (i.e., absolute versus relative) of errors is established in order to understand their impact on this kind of deconvolution approach. Combining both IOP and SIOP uncertainties leads to spread error distributions for each constituent that broadly scale with the

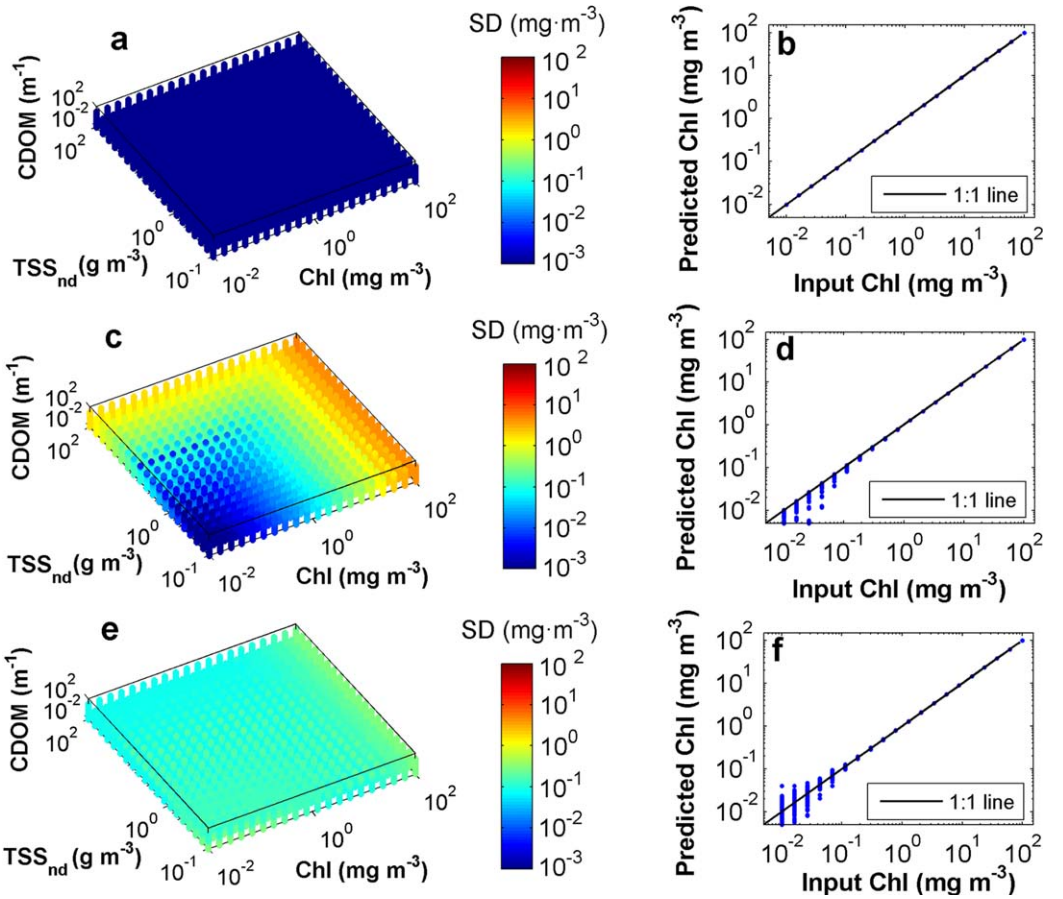

Figure 5. *Chl* standard deviation distributions for the synthetic IOP data set incorporating: (a, b) zero error in both IOPs and SIOPs, (c, d) zero error in IOPs and 5% error in SIOPs, and (e, f) $\sigma = \pm 0.0025$ m^{-1} error in IOPs and zero error in SIOPs.

magnitude of the corresponding constituent concentration (Figures 6a, 6c, and 6e). Interestingly, the effect of combining IOP and SIOP errors is for offset errors to be reasonably uniformly spread around the 1:1 line and to become significant only at low concentrations of each constituent (Figures 6b, 6d, and 6f). Combining IOP and SIOP errors in the deconvolution method results minimum and maximum spread (σ) and offset errors shown in Table 1. Both spread and offset errors are maximal when associated input concentrations are highest. So although these are in some cases large absolute values, in relative terms they are all less than 10% and in many cases much less than 1%. On the other hand, the apparently small values of minimum spread errors in Table 1 correspond to low input concentrations and actually represent significant relative errors, up to almost an order of magnitude in the case of *Chl*. Overall, it seems reasonable that relative errors in constituent retrieval should increase as the contribution of that constituent to the formation of the optical signals diminishes. The retrieval of *Chl* at low concentrations appears to be significantly worse than for the other constituents. However, this really reflects the fact that the simulations have been performed for concentration combinations where the contribution of *Chl* to the formation of optical signals is almost insignificant: there is no reason to expect that such small contributions can be efficiently resolved, and this level of performance is therefore entirely within reason.

Table 1
Minimum and Maximum Standard Deviations (σ) and Offset Errors of the Retrieved Variables Obtained From the Inversion of Simulated IOPs

Constituent	Min σ	Max σ	Max offset error
Chl (mg m^{-3})	0.08	5.02	0.47
TSS_{nd} (g m^{-3})	0.047	9.32	0.68
CDOM (m^{-1})	0.0029	1.41	1.28

4.4. Inversion of In Situ IOPs at Sample Depths

The IOP inversion model was applied to in situ AC-9 measurements collected close to the sea surface. Since the SIOPs were previously determined using the same surface water samples, this analysis is not a rigorous test of model performance but does allow determination of how well the single set of linearly derived SIOPs represents the

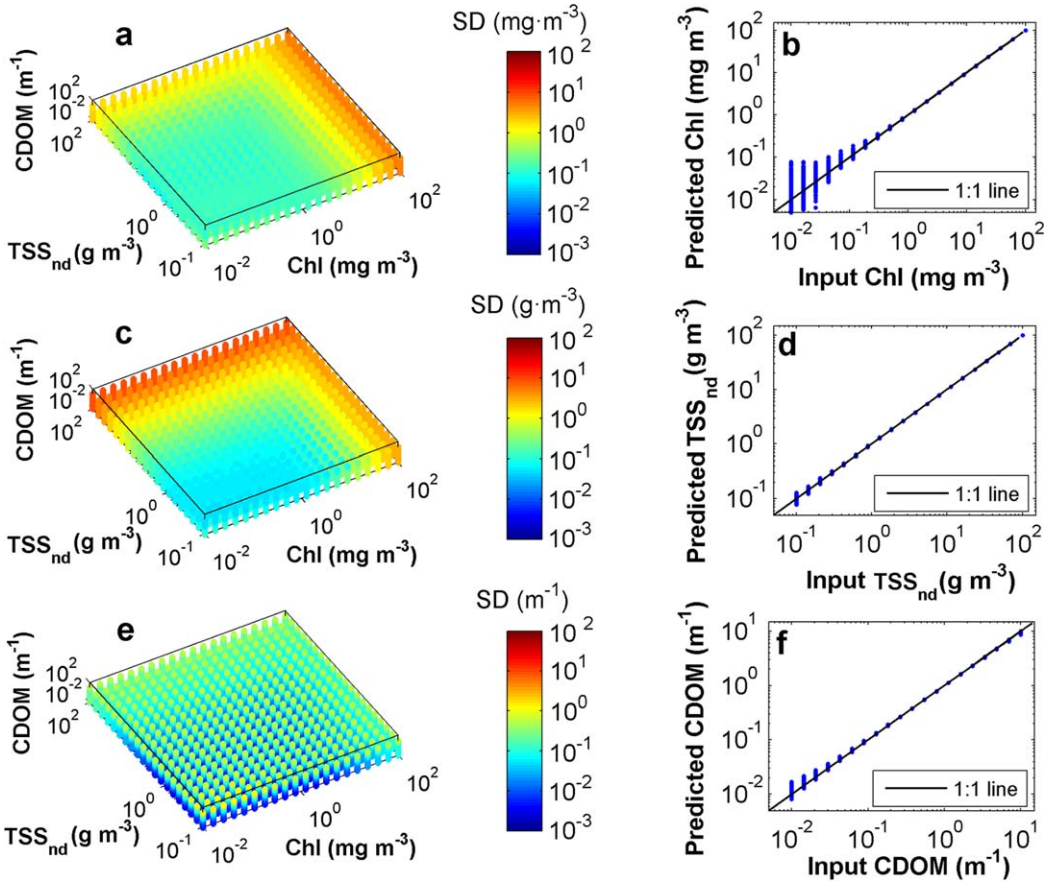

Figure 6. Spread and offset error distributions for (a, b) *Chl*, (c, d) TSS_{nd}, and (e, f) CDOM for IOP inversions with $\sigma = \pm 0.0025$ m^{-1} error in IOPs and 5% error in SIOPs.

optical properties of the data set. As offshore and onshore stations were considered as Case I and Case II waters, respectively, the inversion procedure was implemented separately to both data subsets. For Case I waters, the term related to TSS_{nd} in equation (6) was neglected, leaving only *Chl* and *CDOM* as the model unknowns. The full set of terms in equation (6) was used in the inversion procedure for Case II waters. The bootstrap method was used to estimate uncertainties in retrieved biogeochemical variables by including random noise with $\sigma = \pm 0.0025$ m^{-1} for the IOPs, using the observed 95% confidence intervals for the SIOPs and repeating each calculation 1,000 times to build statistically sound distributions. Figures 7 and 8 show the comparison of retrieved and measured biogeochemical variables for Case I and II water types. The error bars are standard deviations of the bootstrap distributions. For Case I waters (Figure 7) modeled *Chl* and *CDOM* were both distributed around the 1:1 line with RMSE of 0.58 mg^{-3} and 0.008 m^{-1}, respectively. In both cases, the error bars from bootstrapping were generally insufficient to explain the deviation from 1:1 which suggests that either there has been an underestimation in the magnitude of errors in the input IOPs or there is an as yet unknown factor that needs to be accounted for in the inversion procedure. The agreement between modeled and measured variables declined slightly (see RMSE values in Table 2) when the inversion was applied to the optically complex onshore stations (Figure 8). The model tended to simultaneously overestimate *Chl* and underestimate TSS_{nd}, while *CDOM* retrieval was generally closer to the 1:1 line but was also slightly overestimated as its concentration increased. RMSE errors for the retrieval of *Chl*, TSS_{nd}, and *CDOM* using the in situ IOP data set are given in Table 2. Note the increase in the magnitude of the *Chl* and *CDOM* errors and introduction of systematic deviations from the 1:1 line moving from the Case I to Case II model, presumably reflecting the influence of including the additional TSS_{nd} parameterization in the Case II version. The introduction of systematic errors for Case II retrievals, where there appears to be some sort of mutual compensation in the recovery of each parameter, requires particular further attention and is discussed in more detail later.

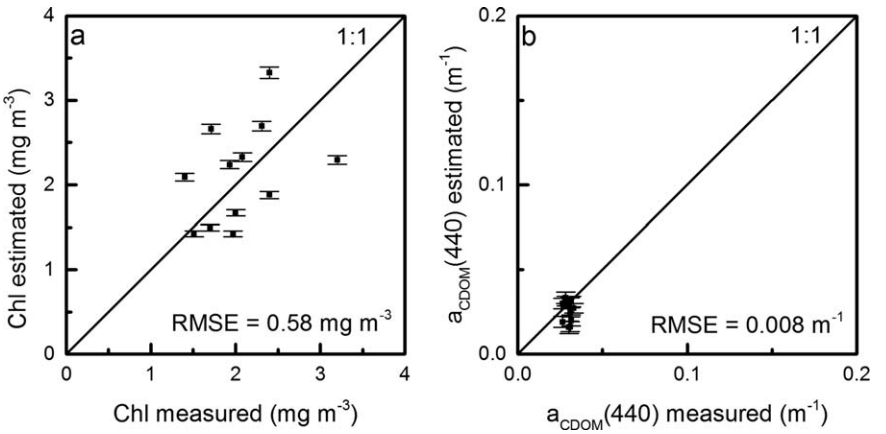

Figure 7. Comparison of retrieved *versus* measured (a) *Chl* and (b) *CDOM* for offshore stations (Case I waters model). The error bars are standard deviations of bootstrap distributions.

4.5. Deconvolution of Vertical IOP Profiles

The inversion model was applied to depth profiles of in situ AC-9 measurements collected at the onshore stations. The retrieved vertical structures of *Chl*, TSS_{nd}, and *CDOM* with associated uncertainties are shown in Figures 9–11. Results from laboratory analyses of discrete water samples (including deep samples not previously used for SIOP generation) are also presented for validation with the modeled constituent concentrations. *Chl* and *CDOM* profiles are broadly consistent with measured values through the water column, though this agreement generally declined for the shallower stations. Measured TSS_{nd} data were only available for surface waters, which therefore precludes the possibility of validating the vertical distributions of this variable. It is interesting to note, however, that the shallower stations show characteristic increases in TSS_{nd} toward the sea bottom, consistent with resuspension of sediment near the sea bed. Furthermore, deeper stations (close to or even over the shelf edge) exhibited a homogeneous vertical distribution and consistently low values of $TSS_{nd} < 0.22$ g m^{-3}, e.g., stations #1, #2, #3, and #6.

5. Discussion

The spectral deconvolution approach developed here is built on a simple four component bio-optical model (water, phytoplankton, mineral or nonbiogenic particles, and *CDOM*) that is conceptually as close to a standard model for Case II as currently exists. The deconvolution method seeks to exploit all of the spectral information that an AC-9 instrument is able to provide and it has been shown that in the case of a perfect data set it is capable of returning essentially perfect estimates of the required biogeochemical

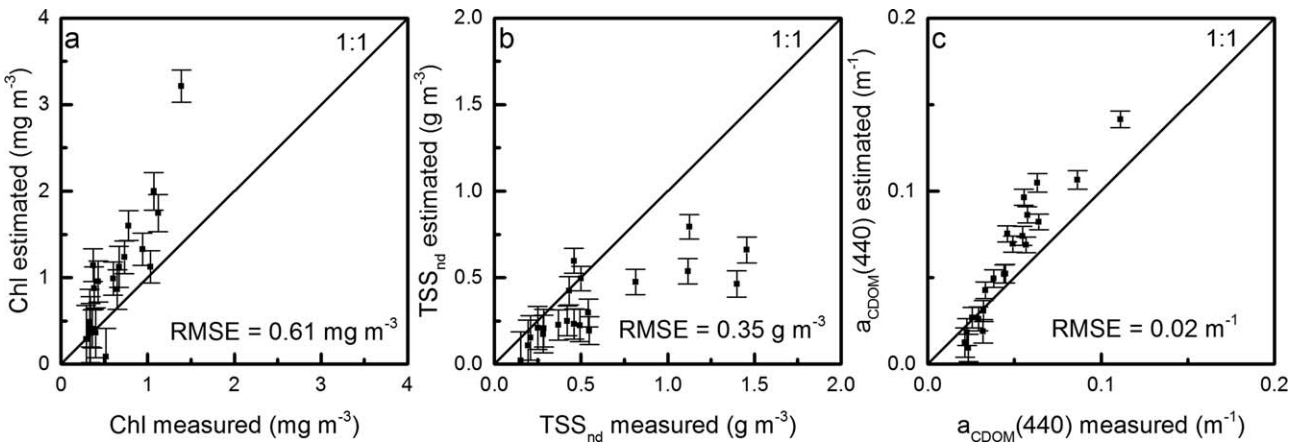

Figure 8. Comparison of retrieved *versus* measured (a) *Chl*, (b) TSS_{nd}, and (c) *CDOM* for onshore stations (Case II waters model). The error bars are standard deviations of bootstrap distributions.

Table 2
RMSE and Percent Absolute Errors Obtained From the Inversion of In Situ AC-9 Measurements of Offshore and Onshore Stations From Ligurian Sea

	RMSE		% Absolute error	
Constituent	Case I (offshore)	Case II (onshore)	Case I (offshore)	Case II (onshore)
Chl (mg m^{-3})	0.58	0.61	24.8	69.3
TSS_{nd} (g m^{-3})		0.35		43.9
CDOM (m^{-1})	0.008	0.02	22.16	34.9

concentrations (Figure 5a). Of course it is expected that real data sets will contain measurement uncertainties, and it has been shown using a synthetic IOP data set that the effect of introducing such uncertainties into the deconvolution process is primarily to introduce a spread error into the results, with offset errors being found to be practically negligible in comparison. If the proposed bio-optical model is a reasonable representation of the natural system, one might hope, therefore, to observe retrieved biogeochemical constituents that have a spread centered on the 1:1 line when plotted against real sample data. Indeed this is the case for the Case I data set (Figure 7) where both *Chl* and *CDOM* retrieved values are scattered around

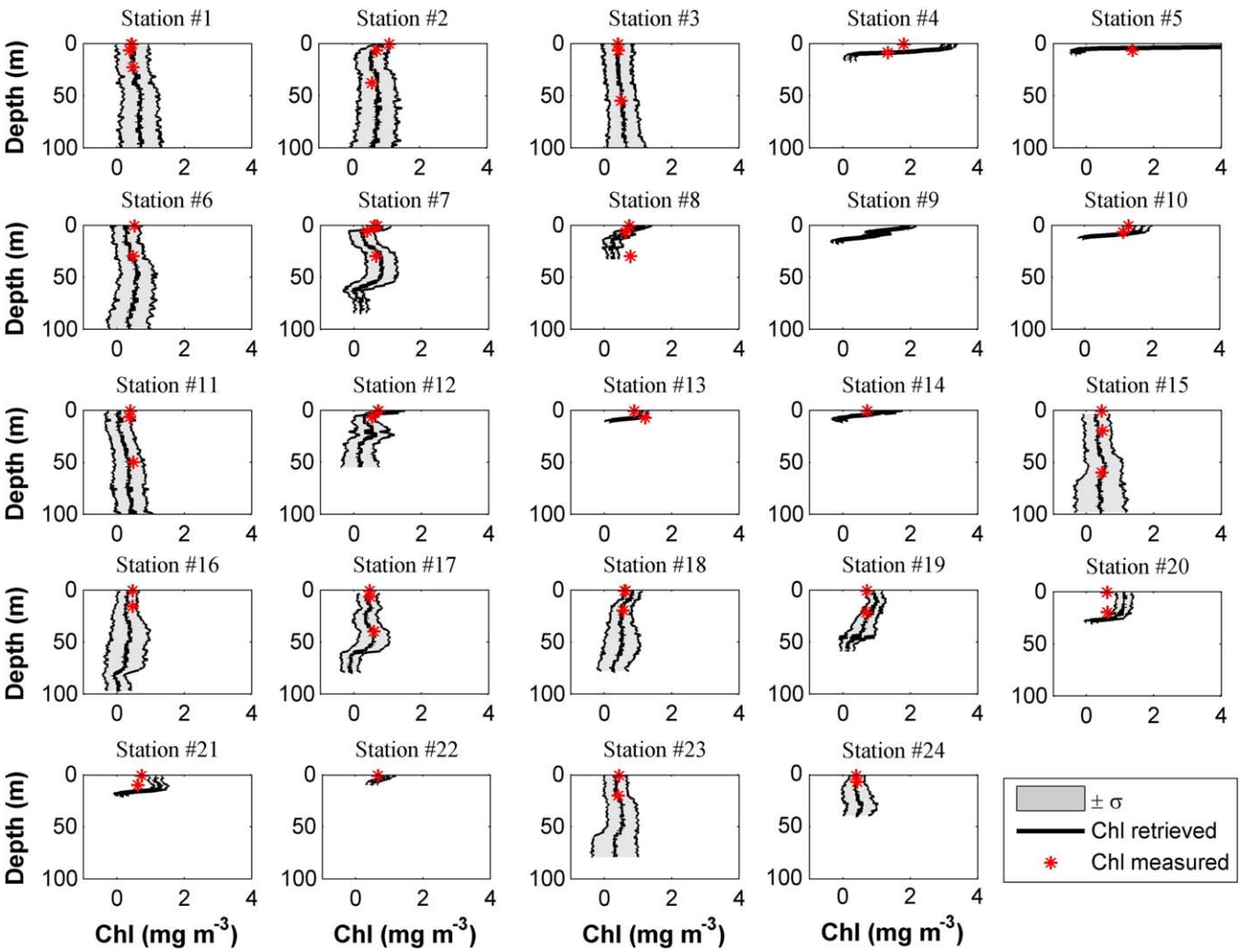

Figure 9. *Chl* depth profiles from onshore stations in the Ligurian Sea retrieved from the inversion of AC-9 measurements. Retrieved values are shown as thick black lines with shadow areas representing bootstrap standard deviations. Red stars indicate results from laboratory analyses of water samples.

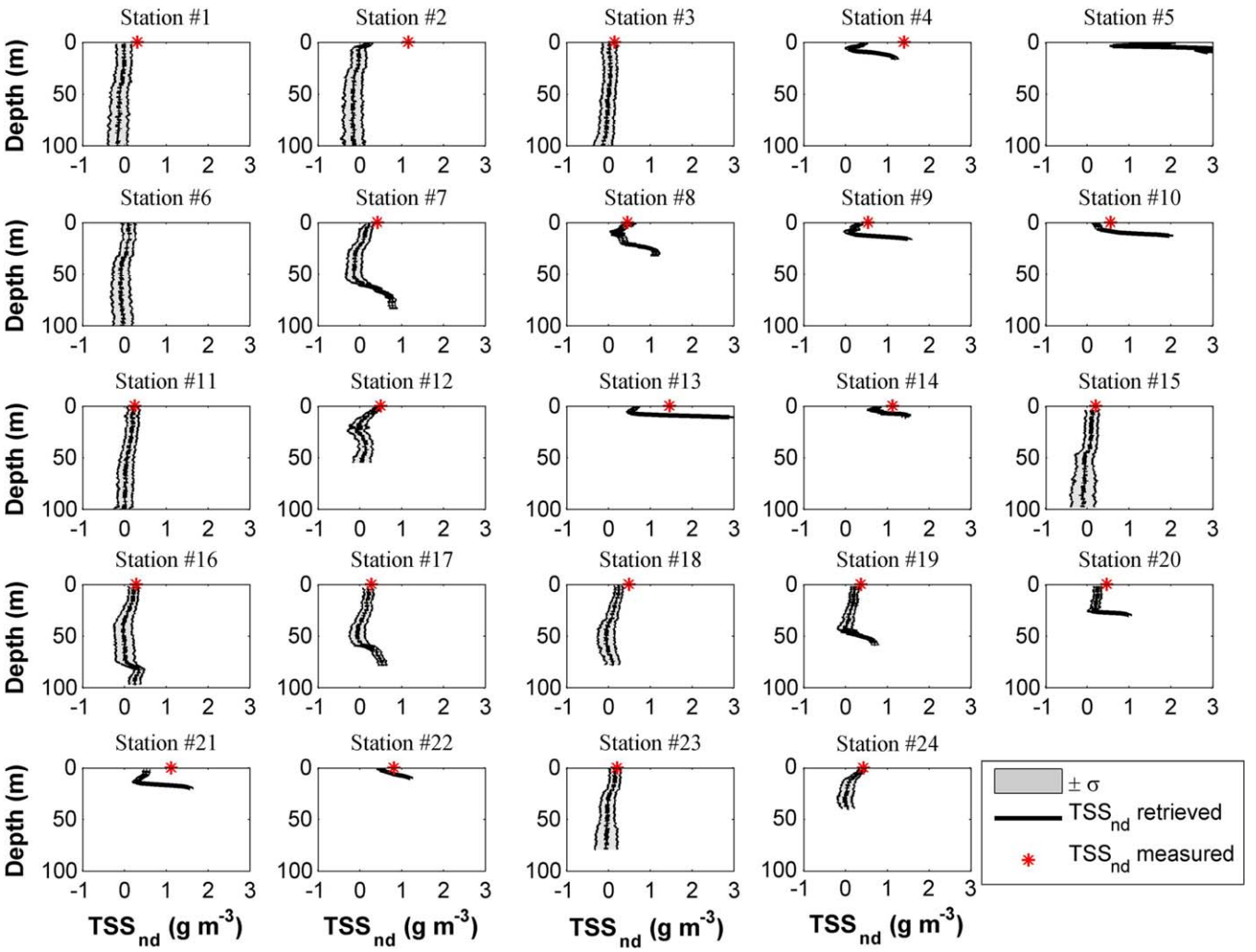

Figure 10. *TSS_{nd}* depth profiles from onshore stations in the Ligurian Sea retrieved from the inversion of AC-9 measurements. Retrieved values are shown as thick black lines with shadow areas representing bootstrap standard deviations. Red stars indicate results from laboratory analyses of water samples.

the 1:1 line. However, the Case II retrievals (Figure 8) deviate from this scenario and show trends toward over and underestimation for different parts of the data set. Given that the deconvolution approach has been shown to perform well for an internally consistent synthetic data set, and to be relatively tolerant to the effects of IOP and SIOP measurement uncertainties, at least in terms of offset errors, the question that arises is: what is the source of these trends away from the 1:1 line within the Case II data set? There are a number of factors that could potentially influence the performance of the deconvolution approach.

The deconvolution approach was built upon an assumption that partial IOPs could be expressed as linear products of the relevant SIOPs and constituent concentrations (equations (3) and (4)). It is well known, however, that there are a variety of factors that may influence such relationships in practice, with the phytoplankton pigment packaging effect perhaps being the best known (Bricaud et al., 1995). The model may therefore be insufficient in its representation of such effects. This is true and a nonlinear version of the approach could be developed but would have to incorporate more sophisticated solution methods. In fact, this is anticipated as an area for future research effort. However, the fact that the Case I results are spread around the 1:1 line suggests that this might not be the missing factor as it would be expected to influence both data sets. The influence of changes in pigment packaging on SIOPs is most likely to be significant for data sets that extend from truly oligotrophic to eutrophic waters and span a broader range of *Chl* concentrations than is the case here.

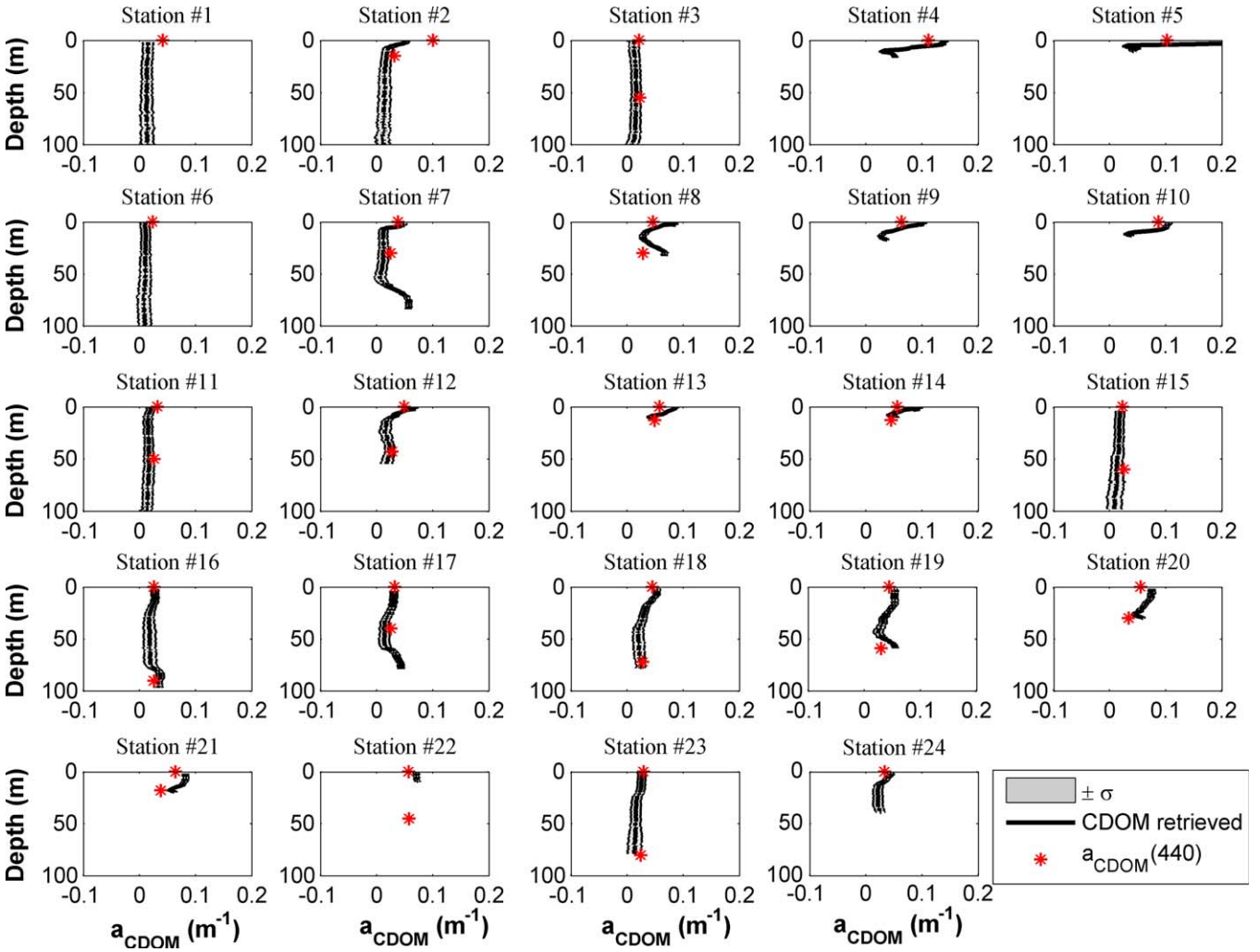

Figure 11. *CDOM* depth profiles from onshore stations in the Ligurian Sea retrieved from the inversion of AC-9 measurements. Retrieved values are shown as thick black lines with shadow areas representing bootstrap standard deviations. Red stars indicate results from laboratory analyses of water samples.

Quantification and propagation of measurement uncertainties of IOPs and SIOPs also may not be optimal. In an earlier study (McKee et al., 2009), the range of measurement uncertainty for AC-9 particulate scattering was found to be significantly greater (∼4X) than the $\sigma = 0.0025$ m^{-1} used here. Increasing this uncertainty estimate would increase the range of the error bars for each constituent retrieval but would not significantly affect the central position of the output distribution. Therefore it does not explain the systematic deviation from 1:1 observed for the Case II data set. The linear regression approach to deriving SIOPs has previously been shown to mitigate the impact of individual uncertainties in IOPs and constituent concentrations (McKee et al., 2014). Errors in measured constituent concentrations have not been directly addressed above but are surely a significant factor in determining the spreads observed in Figures 7 and 8. Again, however, it is unclear how this would generate the systematic deviations observed for the Case II data set.

This then requires a more fundamental problem to be addressed. The underpinning bio-optical model assumes three nonwater components whose optical properties must be consistent across the relevant data sets. This appears to be a reasonable proposition for both the *Chl* and the *CDOM* components as (a) single linear regressions of $a_{ph}(\lambda)$ versus *Chl* and $a_{CDOM}(\lambda)$ versus $a_{CDOM}(440)$ provide high coefficients of determination and (b) the retrieval of both constituents in Case I waters is not biased from the 1:1 line. This leaves the nonbiogenic particulate material as a prime suspect. It was noted above that normalized nonbiogenic detrital scattering spectra showed a broader range of spectral variability than any of the other IOPs. This data is shown in Figure 12. It can be seen that while the $b^*_{nd}(\lambda)$ spectrum (Figure 4f) does capture the most

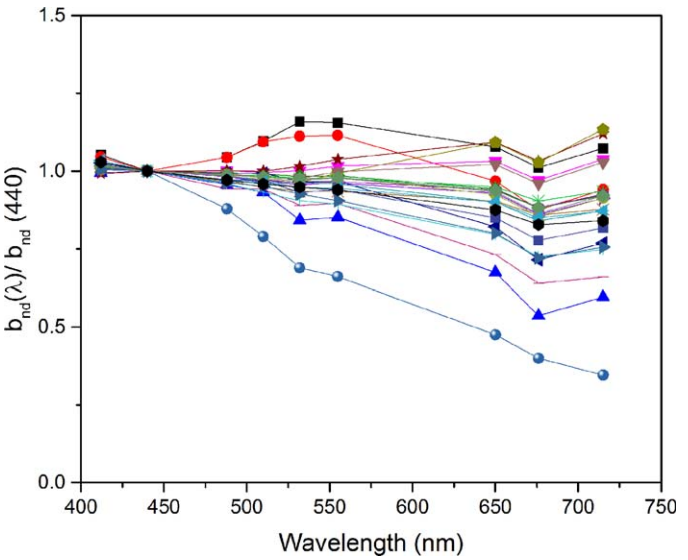

Figure 12. Normalized nonbiogenic detrital scattering spectra for onshore stations. The nonbiogenic detrital scattering coefficient, $b_{nd}(\lambda)$, normalized at 440 nm shows considerable spectral variability that is potentially due to mixing of variable concentrations of two or more subpopulations.

commonly occurring spectral dependency, there is in fact a fairly wide range of spectral variability in this parameter that is not adequately addressed by a single SIOP spectrum. Considering the location of Case II stations and the position of the Arno plume (Figures 1b and 1d), it is possible that there are two (possibly more) nonbiogenic particle types in this region perhaps corresponding to plume and benthic sediment populations. Failure to adequately parameterize this level of population complexity has the potential to disrupt the retrieval of not only TSS_{nd} but also *Chl* and *CDOM* through compensation effects.

6. Conclusions

The conceptual framework of a novel and simple spectral deconvolution approach has been developed and shown to perform well in theory with idealized data and within quantifiable boundaries for data subject to realistic measurement uncertainties. For both Case I and Case II waters, the approach returns estimates of biogeochemical variables that are broadly consistent with the RMSE predictions from the earlier analysis of synthetic data. However, the performance in Case II waters is marred by apparent tendencies to deviate from the 1:1 line that are inconsistent with the synthetic data set predictions. The most likely source of unforeseen error is in the parameterization of the nonbiogenic particle population which in this case is potentially influenced by the presence of material associated with the River Arno plume as well as marine sediments. While the overall model performance is encouraging in terms of RMSE errors, and provides potentially valuable new capability for converting IOP profiles into biogeochemical depth distributions, this study highlights the need to fully capture all of the optically significant and distinct components in a given system. The spectral deconvolution approach developed here could easily accommodate extension of the simple four component model to include additional components. Adding further spectral IOP information through, e.g., moving from AC-9 to AC-S data (9 to 70+ wavelengths) could potentially extend the capacity to resolve such additional components. However, the limiting factor is likely to be ability to determine the SIOPs of additional components. The IOP and constituent partitioning approach used in this study is less easily extended to include resolution of additional components. Development of libraries of SIOPs for naturally occurring sub-populations and generally developing a better understanding of the true variability in SIOPs are both important future steps that would support further development of this type of deconvolution approach and facilitate transition from local as at present to global applicability in the future.

Acknowledgments
The authors thank the captain and crew of the R.V. Alliance for help and support in the collection of data, and our colleagues and friends from the BP09 cruise science team who kindly made data sets available. The paper is dedicated to the memory of our friend and mentor, Chuck Trees, who sadly passed away during the final stages of preparation of this manuscript. Chuck instigated this research and brought together all of the people who contributed to this work. He is greatly missed and we are grateful for his leadership, enthusiasm, and generosity. This work was support by award of a NERC Advanced Fellowship (NE/E013678/1) to McKee. M. Ramírez-Pérez was supported by a fellowship from the Spanish Ministry of Economy and Competitiveness (EEBB-1–15-09678). Authors declare no conflicts of interest. Data supporting the conclusions can be found in PANGAEA database (https://doi.org/10.1594/PANGAEA.880523).

References

Astoreca, R., Doxaran, D., Ruddick, K., Rousseau, V., & Lancelot, C. (2012). Influence of suspended particle concentration, composition and size on the variability of inherent optical properties of the Southern North Sea. *Continental Shelf Research*, *35*, 117–128. https://doi.org/10.1016/j.csr.2012.01.007

Babin, M., & Stramski, D. (2002). Light absorption by aquatic particles in the near-infrared spectral region. *Limnology and Oceanography*, *47*, 911–915. https://doi.org/10.4319/lo.2002.47.3.0911

Babin, M., & Stramski, D. (2004). Variations in the mass-specific absorption coefficient of mineral particles suspended in water. *Limnology and Oceanography*, *49*, 756–767. https://doi.org/10.4319/lo.2004.49.3.0756

Bengil, F., McKee, D., Besiktepe, S. T., Sanjuan Calzado, V., & Trees, C. (2016). A bio-optical model for integration into ecosystem models for the Ligurian Sea. *Progress in Oceanography*, *149*, 1–15. https://doi.org/10.1016/j.pocean.2016.10.007

Boss, E., Collier, R., Larson, G., Fennel, K., & Pegau, W. S. (2007). Measurements of spectral optical properties and their relation to biogeochemical variables and processes in Crater Lake, Crater Lake National Park, OR. *Hydrobiologia*, *574*, 149–159. https://doi.org/10.1007/s10750-006-2609-3

Boss, E., Taylor, L., Gilbert, S., Gundersen, K., Hawley, N., Janzen, C., et al. (2009). Comparison of inherent optical properties as a surrogate for particulate matter concentration in coastal waters. *Limnology and Oceanography: Methods*, *7*, 803–810. https://doi.org/10.4319/lom.2009.7.803

Boss, E., Twardowski, M. S., & Herring, S. (2001). Shape of the particulate beam attenuation spectrum and its inversion to obtain the shape of the particulate size distribution. *Applied Optics*, *40*(27), 4885–4893. https://doi.org/10.1364/AO.40.004885

Bricaud, A., Babin, M., Morel, A., & Claustre, H. (1995). Variability in the chlorophyll-specific absorption coefficients of natural phytoplankton: Analysis and parameterization. *Journal of Geophysical Research: Oceans*, *100*(C7), 13321–13332. https://doi.org/10.1029/95JC00463

Bricaud, A., Morel, A., & Prieur, L. (1983). Optical efficiency factors of some phytoplankters. *Limnology and Oceanography*, *28*, 816–832. https://doi.org/10.4319/lo.1983.28.5.0816

Brown, I. C., Cunningham, A., & McKee, D. (2007). *An approach to determining shelf seawater composition by inversion of in situ inherent optical property measurements*. Paper presented at Oceans 2007 Europe International Conference, Aberdeen. https://doi.org/10.1109/OCEANSE.2007.4302313

Davison, C., & Hinkley, V. D. (1997). *Bootstrap methods and their application*. Cambridge, UK: Cambridge University Press.

Eisner, L. B., Twardowski, M. S., Cowles, T. J., & Perry, M. J. (2003). Resolving phytoplankton photoprotective: Photosynthetic carotenoid ratios on fine scales using in situ spectral absorption measurements. *Limnology and Oceanography*, *48*, 632–646. https://doi.org/10.4319/lo.2003.48.2.0632

Ferrari, G. M., & Tassan, S. (1999). A method using chemical oxidation to remove light absorption by phytoplankton pigments. *Journal of Phycology*, *35*, 1090–1098.

Gallegos, C. L., & Neale, P. J. (2002). Partitioning spectral absorption in case 2 waters: Discrimination of dissolved and particulate components. *Applied Optics*, *41*(21), 4220–4233. https://doi.org/10.1364/AO.41.004220

Gardner, W. D., Blakey, J. C., Walsh, I. D., Richardson, M. J., Pegau, S., Zaneveld, J. R. V., et al. (2001). Optics, particles, stratification and storms on the New England continental shelf. *Journal of Geophysical Research: Oceans*, *106*, 9473–9497. https://doi.org/10.1029/2000JC900161

Groundwater, H., Twardowski, M., Dierssen, H., Sciandre, A., & Freeman, S. (2012). Determining oceanic particle size distributions and particle composition: A new SEM-EDS protocol with validation and comparison to other methods. *Journal of Atmospheric and Oceanic Technology*, *29*, 433–449. https://doi.org/10.1175/JTECH-D-11-00026.1

Hill, P. S., Boss, E., Newgard, J. P., Law, B. A., & Milligan, T. G. (2011). Observations of the sensitivity of beam attenuation to particle size in a coastal bottom boundary layer. *Journal of Geophysical Research: Oceans*, *116*, C02023. https://doi.org/10.1029/2010JC006539

Huot, Y., Brown, C. A., & Cullen, J. J. (2007). Retrieval of phytoplankton biomass from simultaneous inversion of reflectance, the diffuse attenuation coefficient, and Sun-induced fluorescence in coastal waters. *Journal of Geophysical Research: Oceans*, *112*, C06013. https://doi.org/10.1029/2006JC003794

Kirk, J. T. O. (1994). *Light and photosynthesis in aquatic ecosystems* (2nd ed.). Cambridge, UK: Cambridge University Press.

Lee, Z., Lance, V. P., Shang, S., Vaillancourt, R., Freeman, S., Lubac, B., et al. (2011). An assessment of optical properties and primary production derived from remote sensing in the Southern Ocean (SO GasEx). *Journal of Geophysical Research: Oceans*, *116*, C00F03. https://doi.org/10.1029/2010JC006747

Lefering, I., Röttgers, R., Weeks, R., Connor, D., Utschig, C., Heymann, K., et al. (2016). Improved determination of particulate absorption from combined filter pad and PSICAM measurements. *Optics Express*, *24*, 24805–24823. https://doi.org/10.1364/OE.24.024805

Loisel, H., Stramski, D., Mitchell, B. G., Fell, F., Fournier-Sicre, V., Lemasle, B., et al. (2001). Comparison of the ocean inherent optical properties obtained from measurements and inverse modelling. *Applied Optics*, *40*, 2384–2397. https://doi.org/10.1364/AO.40.002384

McKee, D., Chami, M., Brown, I., Calzado, V. S., Doxaran, D., & Cunningham, A. (2009). Role of measurement uncertainties in observed variability in the spectral backscattering ratio. A case study in mineral-rich coastal waters. *Applied Optics*, *48*, 4663–4675. https://doi.org/10.1364/AO.48.004663

McKee, D., & Cunningham, A. (2006). Identification and characterisation of two optical water types in the Irish Sea from in situ inherent optical properties and seawater constituents. *Estuarine Coastal and Shelf Science*, *68*, 305–316. https://doi.org/10.1016/j.ecss.2006.02.010

McKee, D., Röttgers, R., Neukermans, G., Calzado, V. S., Trees, C., AmpoloRella, M., et al. (2014). Impact of measurement uncertainties on determination of chlorophyll-specific absorption coefficient for marine phytoplankton. *Journal of Geophysical Research: Oceans*, *119*, 9013–9025. https://doi.org/10.1002/2014JC009909

Morel, A. (1974). Optical properties of pure water and pure seawater. In N. G. Jerlov & E. S. Nielsen (Eds.), *Optical aspects of oceanography* (pp. 1–14). New York, NY: Academic Press.

Morel, A. (1988). Optical modeling of the upper ocean in relation to its biogenous matter content (case 1 waters). *Journal of Geophysical Research: Oceans*, *93*(C9), 10749–10768. https://doi.org/10.1029/JC093iC09p10749

Nelson, N. B., Siegel, D. A., & Michaels, A. F. (1998). Seasonal dynamics of colored dissolved material in the Sargasso Sea. *Deep Sea Research Part I: Oceanographic Research Papers*, *45*, 931–957. https://doi.org/10.1016/S0967-0637(97)00106-4

Neukermans, G., Loisel, H., Mériaux, X., Astoreca, R., & McKee, D. (2012). In situ variability of mass-specific beam attenuation and backscattering of marine particles with respect to particle size, density, and composition. *Limnology and Oceanography*, *57*, 124–144. https://doi.org/10.4319/lo.2012.57.1.0124

Pegau, W. S., Gray, D., & Zaneveld, J. R. V. (1997). Absorption and attenuation of visible and near-infrared light in water: Dependence on temperature and salinity. *Applied Optics*, *36*, 6035–6046. https://doi.org/10.1364/AO.36.006035

Pope, R., & Fry, E. (1997). Absorption spectrum (380–700 nm) of pure water. II. Integrating cavity measurements. *Applied Optics*, *36*, 8710–8723. https://doi.org/10.1364/AO.36.008710

Röttgers, R., & Doerffer, R. (2007). Measurements of optical absorption by chromophoric dissolved organic matter using a point-source integrating-cavity absorption meter. *Limnology and Oceanography: Methods*, *5*, 126–135. https://doi.org/10.4319/lom.2007.5.126

Röttgers, R., Häse, C., & Doerffer, R. (2007). Determination of the particulate absorption of microalgae using a point-source integrating-cavity absorption meter: Verification with a photometric technique, improvements for pigment bleaching and correction for chlorophyll fluorescence. *Limnology and Oceanography: Methods*, *5*, 1–12. https://doi.org/10.4319/lom.2007.5.1

Röttgers, R., Schönfeld, W., Kipp, P. R., & Doerffer, R. (2005). Practical test of point-source integrating cavity absorption meter: The performance of different collector assemblies. *Applied Optics*, *44*, 5549–5560. https://doi.org/10.1364/AO.44.005549

Schofield, O., Bergmann, T., Oliver, M. J., Irwin, A., Kirkpatrick, G., Bissett, W. P., et al. (2004). Inversion of spectral absorption in the optically complex coastal waters of the Mid-Atlantic Bight. *Journal of Geophysical Research: Oceans*, *109*, C12S04. https://doi.org/10.1029/2003JC002071

Smith, R. C., & Baker, K. S. (1978). The bio-optical state of ocean waters and remote sensing. *Limnology and Oceanography*, *23*, 247–259.

Stramski, D., & Morel, A. (1990). Optical properties of photosynthetic picoplankton in different physiological states as affected by growth irradiance. *Deep Sea Research Part A. Oceanographic Research Papers*, *37*, 245–266. https://doi.org/10.1016/0198-0149(90)90126-G

Stramski, D., Reynolds, R. A., Kahru, M., & Mitchell, B. G. (1999). Estimation of particulate organic carbon in the ocean from satellite remote sensing. *Science*, *285*, 239–241. https://doi.org/10.1126/science.285.5425.239

Strömbeck, N., Candiani, G., Giardino, C., & Zilioli, E. (2004). *Water quality monitoring of Lake Garda using multi-temporal data*. Paper presented at MERIS User Workshop (ESA SP-549, May 2004), Frascati, Italy, November 10–13, 2003.

Torrecilla, E., Stramski, D., Reynolds, R. A., Millan-Nunez, E., & Piera, J. (2011). Cluster analysis of hyperspectral optical data for discriminating phytoplankton pigment assemblages in the open ocean. *Remote Sensing of Environment*, *115*, 2578–2593. https://doi.org/10.1016/j.rse.2011.05.014

Twardowski, M., Zhang, X., Vagle, S., Sullivan, J., Freeman, S., Czerski, H., et al. (2012). The optical volume scattering function in a surf zone inverted to derive sediment and bubble particle subpopulations. *Journal of Geophysical Research: Oceans*, *117*, C00H17. https://doi.org/10.1029/2011JC007347

Twardowski, M. S., Boss, E., Macdonald, J. B., Pegau, W. S., Barnard, A. H., & Zaneveld, J. R. V. (2001). A model for estimating bulk refractive index from the optical backscattering ratio and the implications for understanding particle composition in Case I and Case II waters. *Journal of Geophysical Research: Oceans*, *106*(C7), 14129–14142. https://doi.org/10.1029/2000JC000404

Twardowski, M. S., Lewis, M., Barnard, A., & Zaneveld, J. R. V. (2005). In-water instrumentation and platforms for ocean color remote sensing applications. In R. Miller, C. Del Castillo, & D. McKee (Eds.), *Remote sensing of coastal aquatic waters* (pp. 69–100). Dordrecht, the Netherlands: Springer.

Zaneveld, J. R. V., Kitchen, J. C., & Moore, C. (1994). Scattering error correction of reflecting-tube absorption meters. In J. S. Jaffe (Ed.), *Proceedings of ocean optics XII* (Vol. 2258, pp. 44–55). Bergen, Norway: SPIE.

Zheng, G., & Stramski, D. (2013). A model for partitioning the light absorption coefficient of suspended marine particles into phytoplankton and nonalgal components. *Journal of Geophysical Research: Oceans*, *118*, 2977–2991. https://doi.org/10.1002/jgrc.20206